Available online at www.sciencedirect.com
SCIENCE DIRECT®
Journal of Nuclear Materials 323 (2003) 8–17
journal of nuclear materials
www.elsevier.com/locate/jnucmat

Uranium oxide weathering: spectroscopy and kinetics

R.A. Schueneman [a], A.I. Khaskelis [a], D. Eastwood [a], W.J. van Ooij [b], L.W. Burggraf [a,*]

[a] Department of Engineering Physics, Air Force Institute of Technology, WBAFB, OH 45433, USA
[b] Department of Chemical and Material Engineering, University of Cincinnati, Cincinnati, OH 45221, USA

Received 23 April 2003; accepted 14 July 2003

Abstract

Particles of UO_{2+x} ($x \cong 0.16 \pm 0.06$) exposed to the atmosphere react by oxidation and formation of complexes (hydrates, hydroxides and carbonates). Surface reactions alter and erode the UO_2 particles. This paper outlines results for measurements of oxidation rates on uranium oxide particles using in situ photoluminescence spectroscopy (PL), X-ray photoelectron spectroscopy (XPS) and secondary ion mass spectrometry (SIMS). Phosphorescence spectra observed during oxidation of UO_{2+x} were attributed to U(VI) in uranyl-type coordination and in octahedral coordination. Uranyl-type spectra formed during wet oxidation of UO_{2+x}, and U(VI) octahedral spectra formed during dry oxidation of UO_{2+x}. The uranyl-type species, although more stable, is more kinetically labile for vacuum reduction than is the octahedral U(VI). Oxidation of U(IV) species are diffusion controlled. Vacuum reduction of uranyl U(VI) in UO_3 follows a field-enhanced cationic diffusion rate law, while re-oxidation follows a diffusion rate law. Post-oxidation core and valence band XPS and SIMS measurements provided qualitative and quantitative measures of uranium oxidation states near uranium oxide surfaces.

PACS: 33.60.Fy; 28.41.K; 79.60; 82.80.M

1. Introduction

During nuclear fuel fabrication or reprocessing stages of a nuclear fuel cycle, it is possible for small particles of uranium oxides to escape into the environment. Also, use of depleted uranium munitions disperses large amounts of uranium oxide particles into the environment. Particles of UO_{2+x} ($x \cong 0.16 \pm 0.06$) exposed to the atmosphere react by oxidation and by formation of complexes (hydrates, hydroxides and carbonates), which alter and erode the uranium dioxide particles. This paper reports measurements of rates of oxidation of uranium dioxide particles in controlled gas environments using in situ phosphorescence spectroscopy. Comparison is made with reduction and re-oxidation of uranium trioxide. X-ray photoelectron spectroscopy (XPS) and secondary ion mass spectrometry (SIMS) were used to measure changes in uranium oxidation state and oxide surface structure.

Uranium dioxide has a fluorite structure, which accommodates large uranium cations by simple cubic packing of oxygen ions with eight-fold coordinated U^{4+} in half of the interstitial sites. The large number of vacant sites in this open structure and the high ionic conductivity due to vacancy diffusion, allows stoichiometric UO_2 to be a particularly active substance (although mechanically a very stable nuclear fuel) in which fission products are readily accommodated in the vacant lattice positions. Because of the importance of defect mobility, impurities generated in the uranium oxide fuel by processing, fission or neutron absorption may also influence oxidation kinetics and mechanisms.

* Corresponding author. Tel.: +1-937 2553636x4507; fax:+1-937 2552921.
E-mail address: larry.burggraf@afit.edu (L.W. Burggraf).

0022-3115/$ - see front matter © 2003 Elsevier B.V. All rights reserved.
doi:10.1016/j.jnucmat.2003.07.003

Oxygen ions are also mobile in the UO_2 structure. In the oxygen excess region (UO_{2+x}), interstitial oxygen ions are in higher concentration than vacancies; in the oxygen-deficient region (UO_{2-x}) oxygen vacancies are dominant. In UO_{2+x}, x interstitial oxygen ions are balanced by x U(VI) cations [1] (uranium in oxidation state VI). At low temperature, the concentration of oxygen vacancies is controlled by impurities. At intermediate temperature, oxygen vacancy concentration changes due to variation of oxygen solubility with temperature in the non-stoichiometric oxide.

Detailed mechanisms by which defect structures of uranium dioxide form higher stoichiometric oxides are not yet completely understood. Current understanding of the low-temperature oxidation of stoichiometric UO_2 involves incorporation of oxygen into voids in the UO_2 fluorite lattice by formation of interstitial defects. It is asserted that these defects are randomly distributed in the oxide for low values of x in UO_{2+x} [2]. During oxidation of stoichiometric UO_2 to UO_{2+x}, with larger values of x oxygen atoms are displaced to create a 2:2:2 cluster with overall shrinkage of the unit cell [3]. An additional oxygen atom enters the fluorite lattice along the [1 1 0] direction from the center of the unoccupied cubic hole. Its presence displaces the two nearest-neighbor oxygen atoms from their normal lattice sites to positions along [1 1 1], leaving two normal oxygen vacancies in the oxygen sub-lattice. Thus, in fluorite-type uranium oxides the structure is mainly determined by the packing of the uranium atoms while the octahedral oxygen lattice is increasingly distorted.

In oxygen rich atmospheres, uranium dioxide surfaces chemisorbed additional oxygen in the form of O_2^- or O^-. Interstitially substituted non-stoichiometric transition regions, with O/U ratios greater than two, are formed between the stoichiometric regions [4]. As oxidation of uranium dioxide proceeds, molecular oxygen continues to adsorb on the oxide surface. Some of the oxygen remains on the surface as chemisorbed O_2^- or O^-, or near the surface as interstitials species. Oxygen can be transported through the oxide lattice in the form of O_2^- or O^- to the reactive oxide interface [4]. The rate-limiting factor to further oxidation is the transport of ionic species across the reacted oxide layer. Anionic diffusion is usually more important than cationic migration because the diffusion coefficient for oxygen is orders of magnitude larger than that for uranium ions. As x approaches 0.25 in UO_{2+x}, these oxygen interstitials can interact, by Coulombic forces, and may cluster around the oxidized uranium ion to form ordered U_4O_9. Change in oxygen coordination from eight to 10 accounts for the ordering observed in the transition from the disordered structure of UO_{2+x} to the superlattice structure of U_4O_9 [2,3]. All of the oxidation products of UO_2 are mixed-valence compounds.

Depending on the conditions, one of three simple kinetic models may describe the rate-limiting process for growth or reduction of a U(VI)-rich layer of thickness x on oxides: first order kinetics, Fick's law of diffusion or promoted Cabrera–Mott diffusion. In a first order kinetics model the initial film thickness, x_0, grows as

$$\ln(x_0 - x) \cong kt. \tag{1}$$

Such a reaction-kinetic model assumes that diffusion is comparatively fast and is not rate limiting. If diffusion dominates the rate, the Fick's law diffusion model together with appropriate boundary conditions describes the reaction kinetics. Fick's law diffusion for an infinite slab surface describes increase of the average oxide thickness, $\bar{x}$, with time, t, according to the proportionality:

$$\bar{x} \propto \sqrt{Dt}, \tag{2}$$

where D is the diffusion coefficient. Another possibility is diffusion promoted by Coulombic gradients, which can be described by a promoted diffusion Cabrera–Mott model:

$$\frac{1}{x} \cong \frac{1}{x_0} - k\ln(t). \tag{3}$$

In this case, impurities alter the charge distribution at the boundary and significantly enhance ion mobility. The bulk diffusion coefficient for oxygen mobility in UO_2 is more than five orders of magnitude larger than the uranium diffusion coefficient (over wide temperature range). However, diffusion at boundaries can be enhanced in oxides by several orders of magnitude for the cations present in excess. Oxidation mechanisms involving surface-charge promoted cation mobility (Cabrera–Mott) produce an inverse logarithmic oxide growth rate (Eq. (3)). The field-enhanced ionic transport accelerates initial oxidation, but is rapidly attenuated with increasing thickness according to this model. When the oxide film is thick, on the order of 1–10 nm, the field is no longer strong enough to induce the metal cations to migrate. We compare kinetic data for oxidation and reduction of uranium oxides to these simple models.

One cannot understand the mechanisms and kinetics of oxidation for particulate UO_2 without addressing the dominant influence of the surface, where defects are more readily formed and mobilized. In addition to surface reactions with oxygen, during weathering of uranium dioxide, the presence of other gasses can change oxidation mechanisms. For example, the uranium dioxide surface structure and the surface permeability to oxygen may be altered by chemisorption of water and carbon dioxide.

Photoluminescence (PL) spectroscopy has enabled us to monitor formation and disappearance of two surface U(VI) oxide clusters on uranium dioxide.

Photoluminescence of the U(VI) as uranyl ion, UO_2^{2+}, is one oxidation indicator, which is well characterized by experiments and theory [5,6,16]. Uranyl-type ions persist even in UO_3 oxides and some 'uranates'. In uranyl bonding each uranium (VI) ion is strongly bound to two uranyl oxygen atoms at distances of about 0.175 ± 0.006 nm and less strongly bound to four oxide oxygen atoms at distances of about 0.23 nm. The latter are bridge atoms linking uranyl ions through equatorial oxygen atoms to give $(UO_2)O_2$ chains, layers and networks. The first species, formed during oxidation in the presence of water vapor, has a photoluminescence signature consistent with uranyl-type bonding. We have made some comparisons of uranyl-type spectroscopy and kinetics on weathered uranium dioxide with uranyl reduction and reformation on uranium trioxide.

There are some U(VI) oxide systems (γ-UO_3 and δ-UO_3) that do not contain the uranyl ion, but they are rare [7,8]. The δ-UO_3 is an obvious case, but it is metastable with respect to other phases, which contain uranyl-type ions. In the δ-UO_3 phase the uranium (VI) ion is in an octahedral site, isomorphous with ReO_3. This oxide structure has a metal atom at the center of an octahedron of oxygen atoms, forming a large open cube having four uranium cations at the corners and twelve connecting oxygen atoms in each edge of the cube. It is closely related to the perovskite structures that have, in addition, a large cation at the center of the cube. When uranium atoms are incorporated in double perovskites as an impurity, the U ions in octahedral sites exhibit a broad red PL emission. We attribute the second species, observed during dry oxidation of uranium dioxide by formation of a narrow red PL emission, to U(VI) ions in octahedral vacancy positions in the UO_{2+x} structure.

2. Experimental procedures

2.1. Photoluminescence (PL) measurements

A Jobin Yvon Spex Horiba Fluorolog-3 double excitation/double emission monochromator spectrofluorometer with pulsed 150 W xenon lamp and phosphorimeter accessory was used for delayed photoluminescence measurements. The pulsed source permitted adequate rejection of source scatter and fluorescence, and PL emission was measured using front face optical configuration to enhance intensity. Because the phosphorescence signal was relatively weak for the uranium dioxide samples, the photomultiplier tube was water-cooled to reduce the dark noise counts and large slit widths, providing a 10 nm bandwidth, were used. Time-resolved luminescence measurements were also made using the Fluorolog-3. Details of photoluminescence measurement conditions and procedures are documented elsewhere [14].

A vacuum system with variable temperature optical cell was used for in situ photoluminescence measurements. The system permits PL measurement of oxidation rates for temperatures between room temperature and 400 °C and gas pressures from 10^{-4} to 700 Torr. Temperatures for the uranium oxide samples were controlled using a Lake Shore 330 temperature controller with platinum resistor. The optical cell was fitted with three quartz windows to permit in situ phosphorescence measurements from both front face and right angle. Uranium oxide powder samples, obtained from CERAC were pressed using a Carver hydraulic press into micromachined tungsten screens. A set of custom dies to press samples were created based on a design used in the group of Yates et al. [22].

2.2. Secondary ion mass spectrometry (SIMS) measurements

Static SIMS measurements were conducted using a Cameca TOF-SIMS IV apparatus. The SIMS instrument uses a three-lens $^{69}Ga^+$ liquid metal ion source for surface scans and high-intensity, low energy Ar^+ source for high resolution depth profiling. Surface scans in the positive and negative ion modes up to 1000 u (atomic mass units) were measured: UO_2 and U_3O_7 oxides gave higher intensities in the positive ion mode and were normalized with integrated U^+ ion peak intensity, whereas UO_3 and U_3O_8 gave higher intensities in the negative ion mode and were normalized with integrated O^- ion peak of each sample. Depth profiling was done using timed argon ion sputtering for 200 s ($\sim$2 nm). Because the samples were prepared from powders, the depth profile data reflect a qualitative trend in the ratio of oxides present on uranium oxide particle surfaces relative to particle interiors.

2.3. X-ray photoelectron spectroscopy (XPS) measurements

The XPS measurements were conducted using a Kratos XSAM Ultra XPS Instrument. This instrument uses a monochromatic aluminum Kα X-ray source (300 W), with a charge compensation system. The accuracy of the binding energy measurements was about 0.1 eV. A carbon 1s internal standard was used to calibrate the energy scale (binding energy is 284.6 eV). The sampling area for a wide area scan was 300 by 700 m with the highest available lateral resolution around 10 μm. For each sample, a low-resolution scan from 0 to 1200 eV and high resolution scans from 0 to 13 eV (valence region) and from 280 to 304 eV (U 4f core level region) were measured in two different locations on the sample. Despite the fact, that angular-dependent XPS measurements are somewhat compromised for rough surfaces, such as pressed powders, they help to reveal changes in

uranium oxidation state and concentration in the oxide as a function of depth. For this research, measurements at 90° and 25° take-off angles were used for variable depth measurements, taking advantage of the nearly exponential decrease of photoelectron escape with depth. The effective photoelectron sample depth is about three times the mean free path length (about 5 nm for a 400 eV photoelectron). At 25° the depth from which photoelectron are sampled is reduced by at least $\sin\Theta = 0.42$ to about 2 nm, the top few monolayers. The nature and morphology of the uranium oxide proved to be very different in these two regions [10].

3. Results and discussion

3.1. Photoluminescence results

Two different U(VI) coordination environments produced by weathering of uranium dioxide were distinguished by their photoluminescence emission spectra and lifetimes. These different emission spectra we attribute to two near-surface U(VI) species having different oxygen coordination, an amorphous uranyl-type coordination and an octahedral bonding environment. Both U(VI) coordination-state signatures are reduced at low oxygen pressure. We have begun to measure rates of formation and decay of both U(VI) PL signatures in uranium oxides. Changes in these PL signatures were correlated with XPS and SIMS spectra.

The uranyl U(VI) PL signature is well known [7–9,11]. Photoluminescence emission spectra for uranium oxide starting materials are shown in Fig. 1. The UO_3 material exhibits the typical uranyl emission spectrum. Uranyl emission peaks for UO_3 were consistent with reports by Hanchar [11] and earlier measurements in our laboratory. Detailed discussion and description of the spectral signature for uranyl U(VI) can be found elsewhere [23]. The UO_{2+x} and U_3O_8 materials used in this study display no discernible uranyl-type emission.

A uranyl-type photoluminescence excitation peak at 423 ± 2 nm and emission intensities around 490, 515 and 535 nm grow with oxidation of uranium dioxide under some weathering conditions, all involving exposure to moist air. The uranyl emission spectrum observed on the surfaces of oxidized UO_{2+x} particles has a less well-defined vibrational structure than for UO_3 particles suggesting that uranyl on UO_{2+x} particles has a more variable bonding environment for than for crystalline uranyl bonding [23]. Some UO_{2+x} weathering kinetics results are shown in Fig. 2. The uranyl-type PL intensity increases differently in time for various weathering temperatures and humid air environments. Elevated temperature accelerates the oxidation process and ultimately the formation of the uranyl-type U(VI). The rates of oxidation of UO_{2+x} in air are apparently linear, but these low-temperature changes are too small to distinguish between kinetic mechanisms. The activation energy for formation of the uranyl-type signature in wet air is approximately 30 ± 10 kJ/mol. This is similar to activation energies for UO_2 oxidation from 21 to 42 kJ/mol reported by Finch and Murakiami [9]. Carbon dioxide in the atmosphere delays formation of the amorphous uranyl-type structure on UO_{2+x}. Our working hypothesis is that hydroxide produced by oxidation of the wet surface accelerates surface hydrolysis (attack on the UO_2 cubic structure) permitting uranyl formation. So, in the presence of large partial pressures of carbon dioxide, erosion of the surface appears to be delayed until the surface carbonic acid is sufficiently titrated to carbonate.

Lifetimes of uranyl-type photoluminescence vary with uranyl coordination environment, as shown in

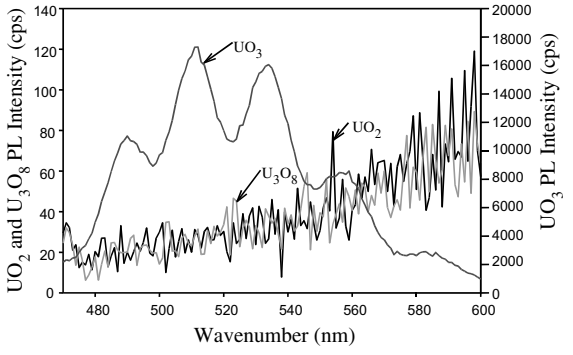

Fig. 1. Lamp corrected delayed photoluminescence emission spectra for reference UO_{2+x}, U_3O_8 and UO_3 materials. Spectra were collected with the following settings: excitation monochromator at 425 nm, delay time 0.15 ms, excitation and emission band pass of 14.7 nm, 100 xenon lamp flashes per data point.

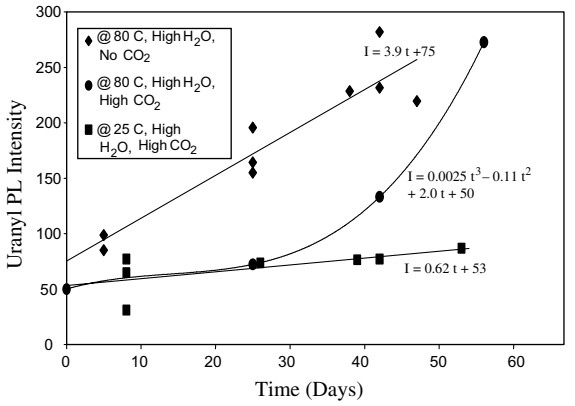

Fig. 2. Uranyl-type U(VI) PL emission intensity versus exposure time for uranium dioxide exposed to various weathering conditions.

Table 1
Comparison of major emission lifetimes for uranyl-type U(VI) phosphorescence signatures in various materials

Samples	Emission lifetime (ms)	R^2 correlation coefficient
Reference materials		
UO_3 particles (NIST)	0.23	0.9999
UO_3 particles (Cerac)	0.14	0.9959
UO_3 glass (MaTech)	0.20	0.9993
Weathered UO_{2+x} particles		
$T = 80$ °C, air, H_2O	0.59	0.9891
$T = 80$ °C, air, H_2O, CO_2	0.36	0.955

Table 1. Photoluminescence lifetimes for the amorphous uranyl-type sites formed on weathered UO_{2+x} are significantly longer than for uranyl structures in UO_3 or uranyl glass. PL lifetimes can help characterize different uranyl-type structures.

Reduction of the uranyl signature on reference UO_3 material with time at reduced oxygen pressure is best fitted by the simple Cabrera–Mott equation; the fits with inverse logarithmic equations are shown in Fig. 3(A) for three different UO_3 samples at room temperature. The Cabrera–Mott constants for reduction are not consistent from sample to sample. This apparent behavior may be a limitation of the vacuum condition at which the experiments were conducted, which contributes to differences in surface preparation. (Experimental pressures were in the range 10^{-3}–10^{-4} Torr.) The activation energy for UO_3 reduction was 19 ± 2 kJ/mol, as determined by the Arrhenius plot for three temperatures between 50 and 110 °C.

Samples of vacuum reduced UO_3 were re-oxidized. As illustrated in Fig. 3(B), a simple diffusion model best describes the re-oxidation process of previously reduced UO_3. Despite the fact that one UO_3 sample was initially reduced at room temperature and another UO_3 sample was reduced at 70 °C, the re-oxidation process displays very similar diffusion controlled behavior. An activation energy of 260 ± 100 kJ/mol was estimated for the diffusion controlled re-oxidation process.

In contrast with wet weathering results, during oxidation studies of UO_{2+x} in dry oxygen environments, no uranyl-type emission signature was observed for any oxidation condition (50–200 °C temperature range, 160–760 Torr partial pressure of oxygen and 92 h maximum duration of exposure). These findings are in good agreement with previous results [12,13,15]. Nor was the 470 nm luminescence emission observed that Winer et al. attributed to F-center defects (an electron on an anion vacancy) formed by oxygen exposure [16,17]. As shown in Fig. 4, a second emission spectrum was observed for UO_{2+x} oxidation in dry oxygen, which has an emission maximum at 695.5 ± 2 nm. The fine structure separation

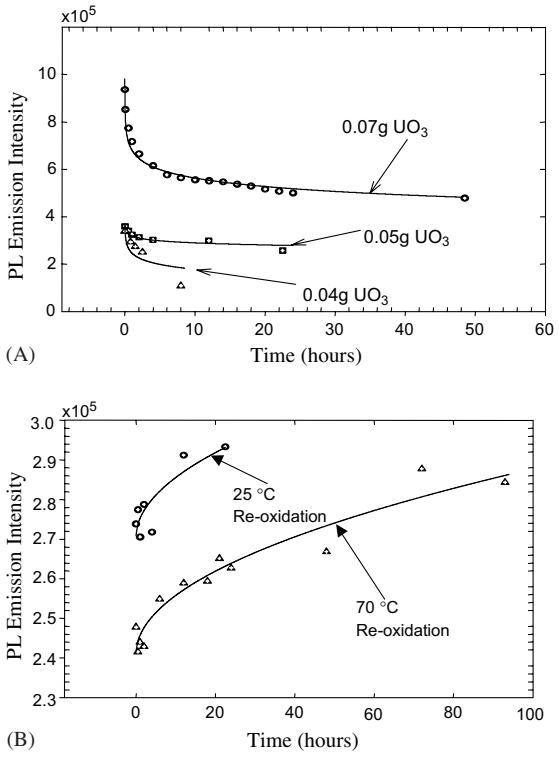

Fig. 3. Uranyl PL emission intensity of UO_3 standard samples. (A) Vacuum reduction of uranyl emission signature with time at milli-Torr pressure and room temperature, best fitted by Cabrera–Mott inverse logarithmic equation. (B) Re-oxidation of reduced UO_3 sample at 760 Torr of oxygen pressure and two different temperatures (25 °C and 70 °C) best fitted by simple diffusion equations: $I = 4815t^{1/2} + 2.7 \times 10^4$ ($R^2 = 0.7429$) at 25 °C and $I = 4682t^{1/2} + 2.4 \times 10^4$ ($R^2 = 0.9256$) at 70 °C.

is approximately 1.9 ± 0.2 nm. We attribute this emission to an octahedral U(VI) species. Based on our initial literature review, this octahedral U(VI) signature has not been characterized before on UO_2 surfaces. Colmenares [6] reported a red PL emission associated with hydrates on oxidized UO_2, which peaks further in the red (~800 nm). The kinetic mechanisms that describe changes between different U(VI) coordination states have not yet been studied. In future studies we plan to explore the kinetics connecting the U(VI) species observed on oxidized UO_{2+x}.

The more rare octahedral U(VI) coordination is less thermodynamically stable than uranyl; however, we find that the uranyl-type state is more labile toward reduction (lower activation energy). The observed red emission persists nearly unchanged for days at 70 °C in less than milli-Torr vacuum, whereas at 150 °C the species is vacuum reduced in a manner similar to reduction of uranyl intensity on UO_3. A caution is warranted in interpreting reduction data. Although the reduction trend

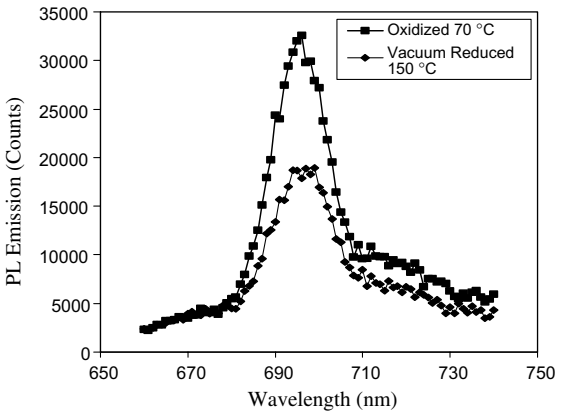

Fig. 4. Unsmoothed, red PL emission spectra for octahedral U(VI) on UO_2 that was oxidized in 760 Torr of oxygen at 70 °C. PL spectra excitation at 425 nm with 14.7 nm bandpass. The U(VI) signature is stable in milli-Torr vacuum for more than one week at 70 °C. At elevated temperature, 150 °C, the emission signature decreases in intensity with time.

generally follows a Cabrera–Mott equation, as shown in Fig. 5(A), a corresponding mechanistic interpretation based on UO_{2+x} is premature. The ultimate surface reduction probably depends on the system pressure that can be achieved. The mechanism for reduction of octahedral U(VI) at elevated temperature may be fit as diffusion process that achieves a steady state determined by the oxygen pressure over the solid, as shown in Fig. 5(B). We have shown that the uranyl-type surface oxide is reduced with Cabrera–Mott type kinetics and reformed by a diffusion mechanism. However, fits to a Cabrera–Mott equation may indicate merely that the process is non-linear and self-limiting rather than specifically involving charge promoted cation mobility. Reduction of the octahedral U(VI) oxide also has been shown to proceed by a diffusion mechanism that saturates, probably due to finite oxygen pressure. Further studies will be completed with a PL spectroscopy cell capable of better vacuum.

3.2. Surface spectroscopy results

Determining the overall oxidation state and the uranium valences is necessary for identification of the products formed during the initial stages of UO_{2+x} dry oxidation. XPS and SIMS surface spectroscopies are sensitive to uranium oxidation states and to near-surface morphology. Uranium oxide state formed as a function of depth in the uranium oxide lattice can be characterized by XPS. However, this technique can not readily distinguish the different coordination environments of U(VI) implied by the PL signatures. XPS was used to determine the overall oxidation state and the uranium valences present near the surface of uranium dioxide.

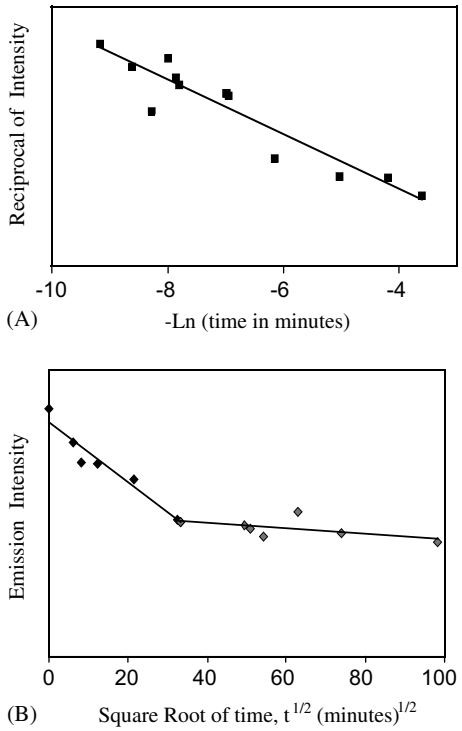

Fig. 5. Decrease of octahedral U(VI) emission intensity during the vacuum reduction of oxidized UO_{2+x} at 70 °C. (A) Octahedral U(VI) reduction is approximately fit to Cabrera–Mott relationship. (B) Octahedral U(VI) reduction is best fit to diffusion equation with reaction limited by steady-state pressure conditions.

Uranium valences were obtained from the intensities and positions of the U $4f_{7/2}$ core level binding energies and valence region of U 5f electrons. By comparing the XPS spectra from the UO_{2+x} weathered samples with spectra for samples of the reference uranium oxides we attempted to distinguish uranium oxidation states. The U $4f_{7/2}$ XPS peak was de-convoluted into three features corresponding to oxidation states U(IV) ('UO_2'), mixed U(IV)–U(VI) in 1:2 ratio ('U_3O_8') and U(VI) ('UO_3') [18]. The typical XPS high resolution spectra of U $4f_{7/2}$ electrons for UO_{2+x} standard baked sample is shown in Fig. 6. We found that all three oxidation states were present in the surface of original UO_{2+x} as a result of storage environment. The XPS spectrum of oxidized UO_{2+x} was interpreted as a conservative system involving these three oxides between room temperature and 150 °C. Near the surface of particles, the UO_2 concentration is nearly constant with increasing temperature, while the UO_3 concentration increases at the expense of U_3O_8 as shown in Fig. 7(A). Deeper in the particle (Fig. 7(B)), the U_3O_8 is approximately constant, while UO_3 concentration increases at the expense of UO_2. Binding energy, line width for U $4f_{7/2}$, composition and atomic

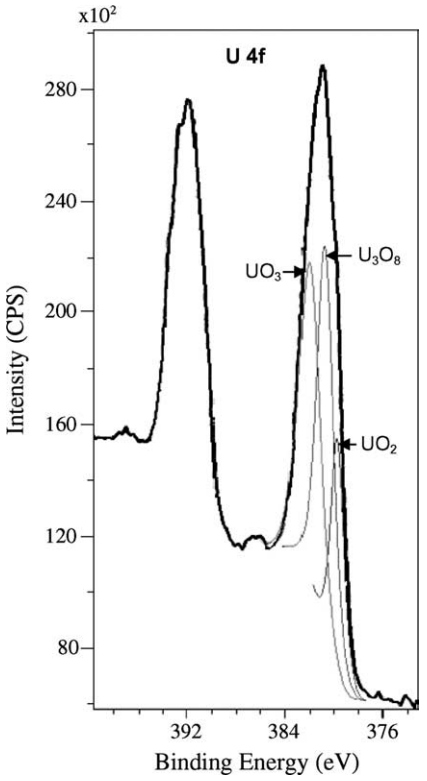

Fig. 6. Curve-fitting of the high resolution XPS U $4f_{7/2}$ spectra of standard UO_2 sample, baked at 120 °C for 12 h period. Spectrum is fitted to XPS spectra of reference materials UO_2, U_3O_8 and UO_3.

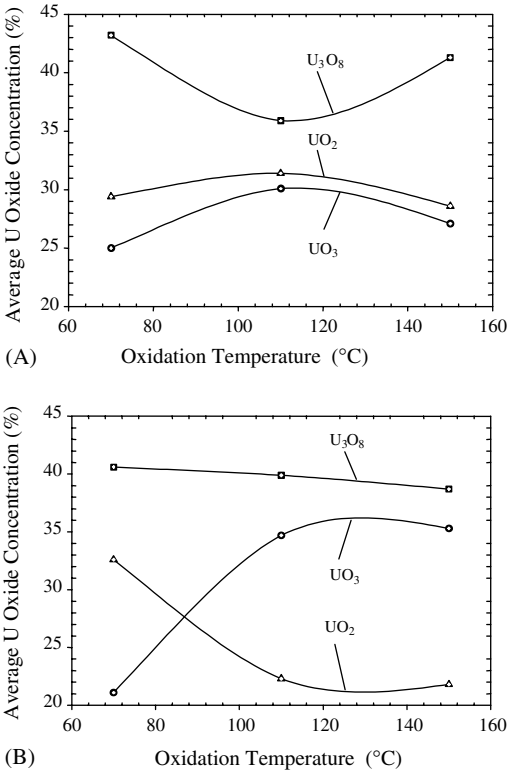

Fig. 7. Comparison of XPS measurements of uranium oxide showing changes in percent concentrations with temperature during UO_{2+x} oxidation for different sampling depths. (A) 25° take-off angle; (B) 90° take-off angle.

concentration for oxidized and untreated UO_{2+x} samples (under oxygen pressure, temperature and duration) at 90° take-off angle are presented in Table 2.

The U $4f_{7/2}$ satellite band spectra and valence band spectra are essential for making conclusion about uranium oxidation state. The satellite band results are not presented in this article. Valence band spectra for UO_{2+x} oxidized dry under different temperature conditions are shown in Fig. 8. The sharp and intense band near the Fermi level (E_f) at ~1.5 eV is attributed to localized U 5f electrons [19]. The broader band at ~5.0 eV is assigned as the O 2p to U bonding band formed from the overlapping oxygen 2p and uranium metal orbital. These results correlate well with the previous findings by Allen et al. [19]. UO_3 powder showed no U 5f intensity ($5f^0$ electronic state), whereas untreated UO_{2+x} powder produced a very intense U 5f signal ($5f^2$ electronic state) shifted ~0.2 eV toward Fermi level. With the temperature increase the U 5f electron intensity decreased, indicating a transfer of the localized U 5f electronic states to the metal–oxygen bonding as the oxygen atoms enter into the lattice. Moreover, the significant increase in metal–oxygen bonding intensity at 200 °C may indicate the formation of a U_3O_8 or other mixed oxide film (although not correlated with results in Fig. 7(B)). This finding well connects with expected UO_{2+x} oxidation process at higher temperatures [20]. The small U 5f shift toward E_f under lower temperatures can be interpreted as beginning of development of the diphasic oxide film of UO_2 and probably U_4O_9 in the form of a heavily doped p-type semiconductor at the surface [19].

The UO_3^- SIMS intensity is consistent with the XPS results. A static SIMS negative mode spectrum of standard baked UO_2 sample is presented in Fig. 9. Each UO_3^- intensity under different experimental conditions was normalized to the O^- ion peak, which is the most intense ion in the negative mode. Two models exist to explain the signal origin, the 'cluster emission model' and the 'recombination model'. Our UO_3^- ion intensities calculations were based on the first model, which assumes that the emitted ion cluster is a small segment of the crystal lattice at the surface. According to Allen et al. [21], the SIMS spectrum may not be used alone in a quantitative manner because it likely measures an equilibrium product of the fragmentation of sputtered cluster species. Instead, SIMS spectra are useful as a

Table 2
Binding energy, line width for U $4f_{7/2}$, composition and atomic concentration for standard and treated UO_2 samples (under oxygen pressure, temperature and duration) at 90° take-off angle

Sample/conditions (P_{O_2}/T/time)	Composition	Binding energy (eV)	FWHM (eV)	Avg.% atomic concentration
UO_2 standard (baked at 120 °C/12h)	UO_2	379.8–380.0	1.31	21.1
	U_3O_8	380.8–381.0	1.62	38.3
	UO_3	382.0–382.1	1.96	40.6
UO_3 standard (baked at 120 °C/12h)	UO_2	Not detected		0.0
	U_3O_8	Not detected		0.0
	UO_3	381.9–382.0	1.41 ± 0.02	100.0
U_3O_8 standard (baked at 120 °C/12h)	UO_2	Not detected		0.0
	U_3O_8	380.5–380.7	1.11	47.9
	UO_3	381.7–381.8	2.17	52.1
UO_2 (760 Torr/150 °C/72h)	UO_2	379.9–380.1	1.45 ± 0.16	21.8
	U_3O_8	381.0–381.1	1.62	38.7
	UO_3	382.0–382.4	2.16 ± 0.05	35.3
UO_2 (760 Torr/110 °C/72h)	UO_2	379.9–380.1	1.51 ± 0.09	22.3
	U_3O_8	381.0–381.1	1.62	39.9
	UO_3	382.2	2.19 ± 0.06	34.7
UO_2 (760 Torr/70 °C/72h)	UO_2	379.9–380.1	1.70 ± 0.03	32.6
	U_3O_8	381.0–381.1	1.62	40.6
	UO_3	382.0–382.1	1.75	21.1

Atomic concentration is a three different lateral measurements average.

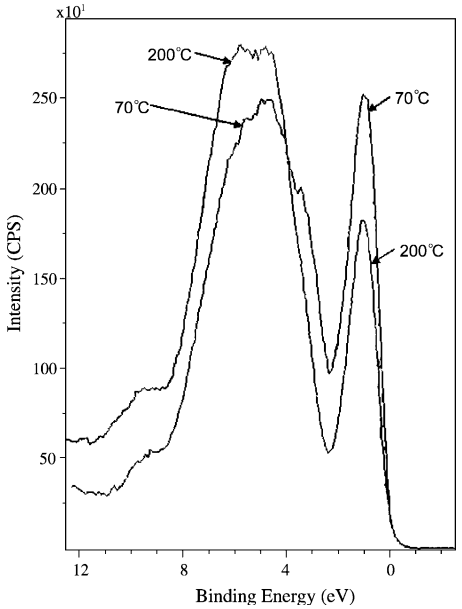

Fig. 8. Valence band changes (90° take-off angle) following oxidation of UO_2 under different temperatures at 0.1 MPa (one atmosphere) oxygen pressure for 72 h.

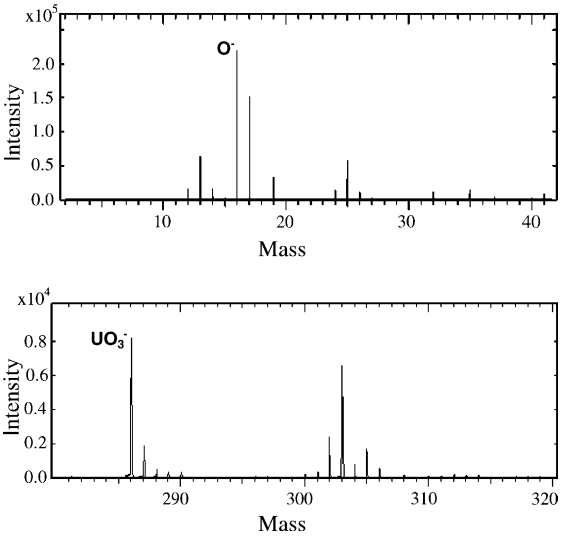

Fig. 9. Static SIMS negative spectrum of standard UO_2 sample, baked at 120 °C for 12 h period.

qualitative technique to understand the chemical environment and uranium/oxygen ratios. Near the UO_2 surface, the U(VI) concentration (measured by SIMS and 25° XPS) increased with temperature to a maximum at about 100 °C, then it decreased as shown in Fig. 10: UO_3 formed more readily at the surface than deeper in the UO_2 at room temperatures, but this is reversed at higher temperature oxidation. These changes reflect a variation in the oxidation mechanism for small changes

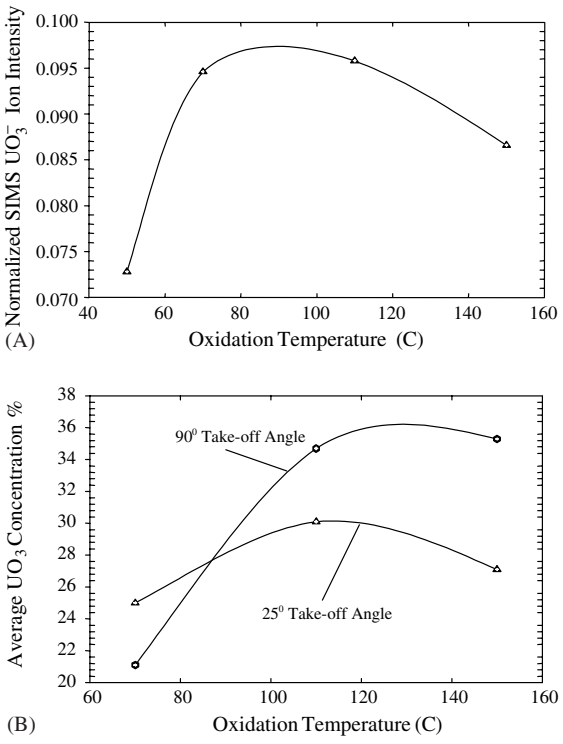

Fig. 10. Comparison of UO_3 concentration changes during UO_2 standard sample oxidation as a function of temperature from SIMS (A) and XPS for two different sampling depths (B).

in temperature. We propose that a thermally activated surface kinetic process dominates at low temperatures and a diffusion mechanism prevails at higher temperatures in the UO_{2+x}. In particular, the initial increase in U(VI) is due to thermal activation of the surface kinetic reaction of molecular oxygen. At higher temperature, above 100 °C, near-surface oxygen ion mobility is activated and oxidation products penetrate deeper into the UO_2 particle. A significant decrease in surface U(VI)/U(IV) ratio occurs for oxygen pressures below 0.05 MPa (half atmosphere). This pressure dependence suggests that the surface kinetic dissociation of molecular oxygen may influence the oxidation mechanism, but this has not yet been studied in detail.

4. Conclusions

Formation of amorphous uranyl-type U(VI) oxides on UO_{2+x} slightly above room temperature in moist air exposures proceeds at different rates depending upon temperature and the presence of carbon dioxide. Uranyl-type U(VI) exhibits longer PL lifetimes on UO_{2+x} than in more crystalline coordination environments. Uranyl-type spectra were not observed for UO_{2+x} oxidation in dry conditions. The rate of vacuum reduction of uranyl-type U(VI) photoluminescence on UO_3 can be well-fitted to a Cabrera–Mott equation, suggesting a reduction mechanism involving Coulomb-enhanced ion mobility in a defected near-surface layer. The activation energy for UO_3 reduction kinetics is approximately 19 kJ/mol. The rate of reformation of the uranyl-type U(VI) photoluminescence on UO_3 by oxidation can be fitted to a diffusion relation. A U(VI) species, not uranyl U(VI), is formed for near-room temperature oxidation of UO_{2+x} in dry oxygen. This species, which we attribute to U(VI) in octahedral coordination, has a narrow phosphorescence emission with a maximum at about 695 nm. The PL, XPS and SIMS signatures for this species increase with room temperature oxidation and are reduced at temperatures above 100 °C. Uranium $4f_{7/2}$ XPS intensities from all U(IV) and U(VI) species from layers within 10 nm of the surface are conservative up to 150 °C, above which they all dramatically decrease. The rates of formation and vacuum reduction measured by in situ photoluminescence, are very different for octahedral U(VI) compared to uranyl-type U(VI). Octahedral U(VI) photoluminescence emission does not reduce in vacuum at 70 °C. At 150 °C it is vacuum reduced, but more slowly than uranyl-type U(VI), by a diffusion mechanism. The uranyl-type state is more labile toward reduction (lower activation energy) even though the uranyl state is thermodynamically more stable than octahedral U(VI). Thus, the number and type of vacancy sites near the surface of UO_{2+x} particles, produced by different processing environments, can influence the types of surface species and surface reaction kinetics controlled by defect formation and transport.

Combining surface spectroscopy techniques and photoluminescence can be a powerful approach for measuring the nature and extent of oxidation on UO_2 particles produced by processing, application and environmental exposure. XPS and SIMS surface spectrometry techniques in combination with photoluminescence measurements give complementary information that should provide a consistent picture of U(VI) formation with temperature for oxidization of UO_{2+x}. Understanding the magnitude of these U(VI) oxides signatures and the rates of their reductive and oxidative titration may be useful to characterize the nature of the uranium oxides and their surface chemistry history.

Acknowledgements

The authors gratefully acknowledge consultation and collaboration with Dr Jeffrey Martin. This work was sponsored in part by Department of Energy, Nuclear Engineering Education Research program.

The views expressed in this report are those of the authors and do not reflect the official policy or position

of the United States Air Force, Department of Defense, or the US Government.

References

[1] C.P. Baird, T.J. Kemp, Program. React. Kinet. 22 (1997) 88.
[2] J. Bruno, Mater. Res. Soc. Symp. Proc. 465 (1997) 491.
[3] G.C. Allen, P.A. Tempest, J. Chem. Soc. Dalton Trans. (1983) 2673.
[4] R.H. Howell, C. Colmenares, T. McCreary, J. Less Common Metals 98 (1984) 267.
[5] H.G. Brittain, D.L. Perry, J. Phys. Chem. 84 (1980) 2630.
[6] C. Colmenares, Prog. Solid State Chem. 15 (1984) 276.
[7] R.G. Denning, in: Electronic Structure and Bonding in Actinyl Ions Structure and Bonding, vol. 79, Springer-Verlag, Berlin, 1992, p. 217.
[8] R.G. Denning, private communication.
[9] R. Finch, T. Murakami, Rev. Mineral. 38 (1999) 91.
[10] S. Van der Berghe, F. Miserque, T. Gouder, B. Gaudreau, M. Verwerft, J. Nucl. Mater. 294 (2001) 168.
[11] J.M. Hanchar, Rev. Mineral. 38 (1999) 499.
[12] R.J. McEachern, P. Taylor, A Review of the Oxidation of Uranium Dioxide at Temperatures below 400 °C, Whiteshell Laboratories, 1997, #AECL-1135.
[13] I. Neretnieks, Mater. Res. Soc. Symp. Proc. 465 (1997) 573.
[14] R.A. Schueneman, Masters thesis AFIT/GNE/ENP/01M-05, Air Force Institute of Technology, 2001.
[15] P. Taylor, R.J. Lemire, D.D. Wood, Nucl. Technol. 104 (1993) 164.
[16] K. Winer, C. Colmenares, F. Wooten, J. Lumin. 31&32 (1984) 357.
[17] Z. Zhang, Doctoral Dissertation, Ohio State University, 1996.
[18] S. Guilbert, M.J. Guitter, N. Barre, M. Gauter-Soyer, P. Trocellier, D. Gosset, Z. Andriambololona, J. Nucl. Mater. 282 (2000) 75.
[19] G.C. Allen, P.M. Tucker, J.W. Tyler, J. Phys. Chem. 86 (1982) 224.
[20] P. Berio, Bull. Soc. Chim. Fr. (1953) 256.
[21] G.C. Allen, I.T. Brown, Nucl. Instr. and Meth. B 88 (1994) 170.
[22] D. Mawhinney, J.A. Rossin, K. Gerhart, J.T. Yates Jr., Langmuir 15 (1999) 4617.
[23] D. Eastwood, J. Martin, L. Burggraf, SPIE Proceeding Environmental Monitoring and Remediation Techniques, vol. 3534, paper 60, 1998, p. 487.